Title
K+-PROTON ELASTIC SCATTERING AT 910 MeV/c; POLARIZATION OF THE RECOIL PROTONS

Authors
Hirsch, Warner
Gidal, George.

Publication Date
1963-08-05

UCRL-10950

University of California

Ernest O. Lawrence Radiation Laboratory

K^+–PROTON ELASTIC SCATTERING AT 910 MeV/c; POLARIZATION OF THE RECOIL PROTONS

Berkeley, California

DISCLAIMER

UCRL-10950

UNIVERSITY OF CALIFORNIA
Lawrence Radiation Laboratory
Berkeley, California

Contract No. W-7405-eng-48

K^+ - PROTON ELASTIC SCATTERING AT 910 MeV/c; POLARIZATION OF THE RECOIL PROTONS

Warner Hirsch and George Gidal

August 5, 1963

K^+ - Proton Elastic Scattering at 910 MeV/c; Polarization of the Recoil Protons

Warner Hirsch and George Gidal

Lawrence Radiation Laboratory
University of California
Berkeley, California

August 5, 1963

ABSTRACT

The Berkeley 30-in. propane bubble chamber was used to study the elastic K^+-proton interaction at 910 MeV/c. This is the region of transition from the isotropy in angular distribution found below 810 MeV/c to the rapidly increasing anisotropy above 1 BeV/c. Results based on 1154 events show that the series $(1 + a \cos \theta_K^{cm})$ can fit the angular distribution with $a = 0.18 \pm 0.05$. Polarization was measured on the secondary proton by using proton-proton and proton-carbon recoils in the liquid of the chamber.

A likelihood function using 53 proton-proton and 41 proton-carbon interactions gave these values for the polarization:

$$\begin{cases} \overline{P}(\ 40 \leq \theta_K^{cm} < \ 70 \text{ deg}) = -\ 0.80 \pm 0.80 \\ \overline{P}(\ 70 \leq \theta_K^{cm} < 100 \text{ deg}) = -\ 0.74 \pm 0.45 \\ \overline{P}(100 \leq \theta_K^{cm} < 140 \text{ deg}) = +\ 0.55 \pm 0.93 \\ \overline{P}(140 \leq \theta_K^{cm} < 160 \text{ deg}) = +\ 0.70 \pm 0.93 \end{cases}$$

The results of a phase-shift analysis incorporating these polarization data are presented.

K^+ - Proton Elastic Scattering at 910 MeV/c; Polarization of the Recoil Protons*

Warner Hirsch† and George Gidal

Lawrence Radiation Laboratory
University of California
Berkeley, California

August 5, 1963

I. INTRODUCTION

The work of Goldhaber et al.[1] indicates that the very-low-energy K^+ - p interaction is characterized by an isotropic angular distribution, by constructive interference between nuclear and Coulomb interactions (therefore by a repulsive nuclear force), and by a negative S-wave phase shift the magnitude of which increases linearly with momentum at least as far as the 640-MeV/c region. A description of the scattering in terms of a $P_{1/2}$ interaction, or a mixture of $P_{1/2}$ and $P_{3/2}$ states, which can also reproduce isotropy, is ruled out by Goldhaber et al. on the basis of the low-energy behavior and the constant character of the angular distribution over this whole momentum region. These results are not in disagreement with the earlier work of Kycia, Kerth, and Baender.[2] At 810 MeV/c, isotropy is still a possible description of the observed angular distribution.[3]

The results of Cook et al.[4,5] at 970, 1170, and 1970 MeV/c show that some anisotropy appears at around 1 BeV/c and increases rapidly in importance. Their 1970-MeV/c data is interpreted with an optical-model approach because most of the angular distribution here appears to be predominantly diffraction scattering.

Our present experiment is to measure the angular distribution in the region of transition, at 910 MeV/c, in order to try to determine, with the aid of polarization measurements on the recoil proton, the nature of the

angular-momentum states involved in the interaction. If good polarization data are available, it is, in principle, possible to distinguish among the mixtures of angular momentum states which can fit the angular distribution. Since proton-carbon scatters have high analyzing power, it is advantageous to conduct the experiment in propane (C_3H_8).

The Berkeley 30-in propane bubble chamber[6] was exposed to a 910-MeV/c separated K^+ beam[7] at the Bevatron. 42,500 pictures were taken. A scan of 19,750 pictures for two-prong scatters yielded 4982 candidate events. These were measured on digitized microscopes and constrained in energy and momentum, using the FOG, CLOUDY, FAIR computer programs,[8] to be elastic K^+-proton interactions.

Of the 4982 events, 1905 had readily identifiable scattered prongs, as indicated by (a) the proton coming to rest in the liquid of the bubble chamber, or (b) the K^+ decaying after scattering, or (c) the K^+ moving in a backward direction with respect to the incoming beam particle. For other events, a scan-table comparison of predicted and observed ionization density and δ-ray formation gave the correct identity of the scattered prongs. These identifications were made after momentum and dip angles of the relevant tracks had been measured.

1154 events were included in the angular distribution after constraint to elastic K^+-proton scattering.

For measurement of the polarization of the recoil proton, all 42,000 pictures were scanned for good K^+-p elastic scatters that were followed by interactions of the recoil protons either on hydrogen or on carbon. Fig. 1 is an example of an elastic K^+p scattering followed by an elastic p-carbon scattering. Good p-hydrogen events had to be coplanar and have the proper opening angle between the scattered protons. Good p-carbon events had to

lie in the acceptable region of a modified Birge-Fowler[9] plot and to show no evidence for an energy loss greater than 50 MeV. Out of 1757 candidate events, 94 met all these criteria (41 p-carbon and 53 p-hydrogen events).

The polarization information was used, with the measured angular distribution, to obtain the best sets of phase shifts to describe K^+-proton elastic scattering.

II. SCANNING

Scanning instructions specify

(a) that an event have two and only two outgoing prongs;

(b) that the incident K^+ enter the bubble chamber within 10° of the average beam direction, and that it have no other interaction prior to the two-prong scatter;

(c) that both scattered prongs not lie to one side of the incident track in both views; that both scattered prongs not go backward with respect to the incident track;

(d) that the scattered prongs be not obviously noncoplanar.

(e) that a track coming to rest in the liquid of the chamber, without decaying, be labelled "proton";

(f) that a track whose ionization becomes less dense abruptly, accompanied by a scatter at this point, be labelled "K^+ decay" unless the kinematics violate this hypothesis;

(g) that a track scattered backward with respect to the incident track be labelled "K^+," and, finally,

(h) that all δ rays on any prong be noted.

Instruction (a) is intended to eliminate a portion of the inelastic interactions on hydrogen or carbon. Item (b) requires that the beam

momentum be up to the average, since tracks scattered on the beam-transport equipment or in the propane itself will have a reduced momentum. Items (c) and (d) are rough elasticity and coplanarity tests. Items (e), (f), and (g) take advantage of the known characteristics of K^+'s and protons to help identify the scattered prongs. Item (h) is used for subsequent identification of prongs. Using the measured momentum value one can differentiate frequently between K^+ and proton on the basis of δ-ray formation. This is also a method of removing π^+ contamination, since the K^+ cannot make δ rays of greater energy than 5 MeV. Scattered tracks less than 3 mm in length were rejected.

For the second portion of this experiment, which involved the measurement of the recoil-proton polarization, an instruction was given to note all interactions on scattered prongs. Another 22,750 pictures were scanned only for such second scatters. The whole film yielded 1757 of these events.

The final angular distribution contains events only from the fully scanned 19,750 picture sample, whereas the polarization measurements use all the available film. The fully scanned rolls of film are interspersed within the total footage to ensure proper sampling.

Of the 4982 candidate events for the angular distribution, 1905 fell under scanning instructions (e), (f), and (g) and thus had their scattered prongs identified. The remaining 3077 events had to be constrained to two elasticity hypotheses corresponding to the possible identity permutation of the scattered tracks ($[K^+, p]$ and $[p, K^+]$).

III. SELECTION CRITERIA

A. Elasticity Criteria

Elastic scattering experiments on hydrogen in a propane chamber are characterized by high background since only one third of the possible interactions take place on free protons. We have three momenta and one energy-conservation conditions on nine measured variables (one momentum and two angles define each track). By using the method of Lagrange undetermined multipliers, a best fit to the elasticity hypothesis and a χ^2 goodness-of-fit estimate are obtained.

We chose a χ^2 cutoff[10] of ten.

To test that this cutoff was appropriate, we plotted the distribution of "quasi-elastic" events, defined as those which had $10 < \chi^2 < 40$ and which also fulfilled the conservation equations after constraint. These are interactions with peripheral protons in carbon. Comparison with the elastic distribution shows that, within statistics, both have the same angular distribution. Thus, choosing our cutoff at $\chi^2 = 10$ does not introduce a bias in the angular distribution.

Having chosen our χ^2 cutoff, we then went back to the scan table and looked at those events with $\chi^2 < 10$ where scattered prongs had not previously been identified. Using the measured momentum from curvature, and compensating for the dip angles of the tracks, we compared the predicted and observed ionization densities to differentiate between the scattered K^+ and proton.

Whenever possible we used the δ rays to aid us. The δ-ray formation is a function of velocity; therefore, a K^+ of given momentum will form more δ rays than a proton of the same momentum. The maximum energy of a δ ray also is velocity dependent. At momenta below 600 MeV/c, for

example, a proton will not create δ rays of sufficient energy to be visible in propane.[11] At 910 MeV/c protons can give δ rays of 0.97 MeV, whereas K^+ can produce δ rays of up to 3.5 MeV.

In some cases it was possible to use range curvature to pick out the K^+. The π^+-proton background interactions can also frequently be detected by using these methods.

By using these three techniques (ionization, δ rays, and range-curvature) we were able to identify 95% of the scattered tracks. Events with unidentified tracks were omitted. These consisted of: (a) those better suited, by observation, to be π^+ than K^+, and (b) those events where tracks were so poor in quality as to be unidentifiable. In the latter class were very steep tracks where the ionization density was unreadable, some kinked tracks where the momentum or range were unmeasurable,[12] and lastly, events falling in regions where temperature gradients caused distortions in the oil between the cameras and the chamber.

Out of the 4982 candidate events sent to the computer, 1448 or 29% passed the constraint tests.

B. π^+ Contamination

The primary beam contamination of π^+ and μ^+ was measured by use of δ rays. First a special scan was made[13] of film from another experiment with known π flux in the same energy region. A count was made of beam-track δ rays with more than 5 MeV, and, separately, of beam-track interactions. These δ rays must come from π or μ, while the interactions must come from π alone. By comparing the results of this count with results from our experiment, we concluded that the combined π and μ background was 8.9 ± 0.5%, on the basis of 307 δ rays greater than 5 MeV on 6735 meters of beam track. The π contamination alone is 5.9 ± 1.2% on the basis of 23 δ

rays greater than 5 MeV found on tracks that subsequently interacted.

To ascertain the maximum possible contamination of the data sample finally selected, we plotted theoretical curves of θ_K (the laboratory scattering angle of the K^+) versus θ_p, and of θ_π versus θ_p (Fig. 2). Good elastic $K^+ - p$ scattering events were placed (before constraint) on this scatter diagram. Their displacements from the θ_K vs θ_p curve and from the θ_π vs θ_p curve were each plotted in histograms shown in Figs. 3a and 3b. Experimental measurement errors in angles are less than 1.0°.

The displaced peak indicates indeed that these events are better fitted to $K^+ - p$ than $\pi^+ - p$ scattering. Yet there is a region, for small θ_K or θ_π, where the theoretical curves approach each other to an angular separation that is of the order of magnitude of the errors. In this region, some overlap is found, and this gives the upper limit to the actual π^+ contamination of our final data.

We have divided the events into those which lie in the region of possible overlap and those which do not. The latter invariably lie at least 1° farther from the π, p curve than the K, p curve. In other words, π^+ contamination is rejected in scanning and by the constraint program; therefore, where no overlap should exist, we have found none. Thus, the background of $\pi^+ - p$ events must exist solely within the overlap region.

If we say that any event lying in the overlap region and within 1° of the θ_π vs θ_p curve could be a $\pi^+ - p$ scattering event, and if we further say that the maximum π contamination of any given set of scattering events is given by the $5.9 \pm 1.2\%$ determined above, then we find a maximum π contamination of our finally selected data of 0.5 %.[14] This is well within the errors due to statistics.

C. Beam Momentum

A plot of measured beam momentum fitted with a Gaussian curve gave the value 910 ± 70 MeV/c. A study of τ decays[15] gave a result (also averaged over the length of the chamber) of 910 ± 60 MeV/c. The momentum loss of the K^+ over the length of the bubble chamber gives a minimum momentum spread of ±50 MeV/c.

The K^+ - p angular distribution is known to vary only slowly with momentum in this region. Nevertheless, some cutoff limits are necessary. We chose 910 ± 100 MeV/c, which is about 1.5 standard deviations.

D. Geometric Criteria

The K^+ - p interaction, assuming a spherically symmetric potential, must be invariant under the rotation of coordinate axes about the incoming beam direction. To test this, the azimuthal angle, ϕ, was plotted. It shows a generally isotropic distribution except for regions at 0, 180, and 360 deg. These are the angles of particles heading almost straight up or down in the chamber. These tracks are hard to see and hard to measure, and we are biased against them. To correct for this, we impose the following acceptable regions (as determined from the experimental ϕ distribution) on the azimuthal angle ϕ:

$$10 \text{ deg} \leq \phi \leq 165 \text{ deg},$$

and

$$190 \text{ deg} \leq \phi \leq 340 \text{ deg}.$$

There was, in addition, a fiducial-region criterion so that all events would lie in easily visible regions of the bubble chamber. This ensured that scanning efficiency would not vary too rapidly with the position of the interaction vertex.

A last criterion specified that the error (after constraint) in $\theta_K^{c.m.}$, the center-of-mass scattering angle of the K^+, be small enough to minimize the chance of events overlapping into adjoining angular distribution boxes. This required an error of less than 6 deg in $\theta_K^{c.m.}$. Only four events were affected.

IV. ANGULAR DISTRIBUTION

In Fig. 4 we show the angular distribution of the 1154 events that met the selection criteria. A cosine power series was fitted to this distribution by a least squares analysis. We find that either

$$\frac{d\sigma}{d\Omega} \propto 1 + (0.18 \pm 0.05) \cos \theta_K^{c.m.} \qquad \text{with} \qquad \chi^2 = 7.2,$$

or

$$\frac{d\sigma}{d\Omega} \propto 1 + (0.20 \pm 0.06) \cos \theta_K^{c.m.} + (0.18 \pm 0.12) \cos^2 \theta_K^{c.m.} \qquad \text{with} \qquad \chi^2 = 4.8,$$

will satisfy the angular distribution. The former is more satisfactory because the addition of the $\cos^2 \theta_K^{c.m.}$ term does not change the coefficient of the $\cos \theta_K^{c.m.}$ term appreciably. And, the coefficient of $\cos^2 \theta_K^{c.m.}$ has an error almost as large as itself.

V. POLARIZATION

From the unknown polarization P_0 produced in a direction $\hat{n}_1$ at the first vertex, the known analyzing power P_1 in direction $\hat{n}_2$ at the second vertex, and $\cos \Phi$, defined as the projection of $\hat{n}_1$ on $\hat{n}_2$, we constructed the likelihood function

$$\mathscr{L}(P_0) \propto \prod_i^k (1 + P_0 P_{1_i} \cos \Phi_i). \qquad (1)$$

The product is over the k second scattering events used, and the ith term is proportional to the probability that the ith event scattered through θ_{1_i}, ϕ_{1_i} at vertex 1, survived undeflected to vertex 2, and scattered there through θ_{2_i}, ϕ_{2_i}.

A set of input values, P_0, then gives a curve with a maximum that defines a most probable value $\overline{P}_0$, averaged over the data under consideration, and a width that defines the uncertainty in this value.

For later combination with a phase-shift analysis, we have used $\mathcal{L}$ to find a value of $\overline{P}_0$ in four intervals of $\theta_K^{c.m.}$, the center-of-mass scattering angle of the K^+.

To be useful for polarization measurements, second scatters must fulfill two conditions: (a) they must occur on proton recoils from an elastic first scatter, and (b) they must be interactions for which polarization measurements have been carried out in some previous experiment.

Condition (a) is necessary for a well-defined polarization state to exist. Condition (b) requires that the analyzing power at the second scatter be known. The analyzing power is equal to the state of polarization that would be induced by such a scatter on an unpolarized beam of protons of the same momentum. This analyzing power has been measured over the entire range of energies accessible to the recoil proton for hydrogen scatters. Proton-carbon scatters have been investigated in the region from perfect elasticity to an energy loss of 50 MeV[9] for most of the accessible energies.

The momentum of the incident proton at the second vertex was well known because this proton had previously been constrained at the first vertex. The momenta of the scattered tracks at the second vertex are often hard to measure because the tracks are short. The angles of such tracks, however, can still be accurately measured.

By convention, the angle of scattering referred to in p-p interactions is the smaller of the two scattering angles, corresponding to the forward hemisphere in the center of mass.

A. Proton-Hydrogen Interactions

Second scatters with two visible outgoing prongs were tested in two ways as being possible elastic p-p scatters.

First, all three tracks were required to be coplanar within certain limits. These cutoff limits were chosen after inspection of the distribution in the value of the triple scalar product of the momentum vectors. This distribution centers at zero with a width of ± 0.05. The limits chosen were ± 0.15.

The second requirement was that the laboratory opening angle of the two outgoing protons be 85 ± 13 deg, as determined from the experimental distribution.

Events which met these two tests and which also were good K^+ - p elastic scatters at the first vertex were given appropriate analyzing power from the graph in the Birge-Fowler paper.[9]

Six requirements have been mentioned for inclusion of an event in the angular distribution. Of these, only the elasticity and beam-momentum restrictions (at the first vertex) were kept for polarization candidates.

B. Proton-Carbon Interactions

The first requirement on prospective p-C scatters was that they should be elastic to within 50 MeV. Only events where the proton momentum and scattering angle fell below the 50 MeV inelasticity line on the Birge-Fowler plot were considered. We also studied the photographs using all available

information, such as momentum, dip angle, measurement errors, and ionization density to estimate the amount of energy loss.

There were a few recoil protons that came to rest in the chamber. Their momentum was known to 3% and their energy loss could be accurately determined. At higher momenta, curvature measurements could be made on the recoil proton. In most cases, however, the amount of inelasticity could not be established. Such events were arbitrarily labelled "elastic." This is reasonable because of the very high relative (300 mb) cross section for elastic scattering in the acceptable Birge-Fowler region.

If an event fell in a region where the analyzing power had not been measured, or could not be found by a short extrapolation, we did not use it. We finally used 41 events.

A bias is introduced by the fact that some of the p-carbon scatters at small angles are really p-hydrogen scatters with proton recoils too short to be seen in propane. The maximum p-p analyzing power of 45% is only half the maximum p-C analyzing power.

To resolve this bias, we plotted the laboratory angular distribution of p-C and p-p scatters as shown in Fig. 5. The p-p angular distribution is isotropic at our energies.[16] We found that portion of our distribution which is indeed a straight line and extended it to 0 deg, to estimate the number of missing p-p scatters.

Not all the p-C scatters in the angular region of the extrapolated line could be p-p, since some configurations would have produced visible recoils.

We estimated that there were 9.8 hidden p-p events in 54 elastic and inelastic p-C scatters. Therefore, each p-C event, if used for the polarization, was assigned a mixed analyzing power, [82% (p-C) + 18% (p-p)].

C. Polarization Analysis

We selected 94 events: 41 p-carbon and 53 p-hydrogen scatters. They are shown plotted in Fig. 6. The ordinate is to be interpreted as the "equivalent number of events of unit analyzing power"; it is the sum $\sum_i (P_{1_i} \cos \Phi_i)$ for all events falling into the same interval of $\theta_K^{c.m.}$. This corresponds to counting up the total effective analyzing power in that interval. It might also be thought of as the number of events that an equivalent counter experiment (of such geometry that $\cos \Phi_i \equiv 1$ and $P_{1_i} \approx 1.00$) might have recorded.

In Fig. 6 we have separated the two classes of second scatters, p-carbon and p-hydrogen. It will be noted that the p-carbon events tend to cluster in the region $\theta_K^{c.m.} < 90$ deg, while the p-hydrogen events tend to lie in the other center of mass hemisphere. This means that, in the laboratory system, p-hydrogen scatters tend to occur with the faster protons, whereas p-carbon scatters tend to be found with the slower protons.

Though the p-p cross section is nearly constant throughout this energy region (70 to 500 MeV), the p-p scatters tend to occur on the faster protons because these lie forward in the chamber and have much longer path lengths with greater likelihood of interaction. The p-C elastic scattering cross section is greatest at the lower energies. The maximum angle of scattering of elastic events of higher energy shrinks to 10°. Unless the plane of such a small scatter is nearly horizontal, it may not be visible. Also, there is 8/3 as much hydrogen as carbon in propane. These circumstances combine to give us fewer p-C events than p-p events although the p-C cross section is larger.

Equation (1) cannot be used for bubble chamber events without including a geometric correction factor.[17] Since the measurement of polarization is

based on an azimuthal asymmetry at the second scattering vertex, we must be able to detect, for a given scattering angle, all azimuthal directions. In other words, protons, scattering in a cone of half angle α about the direction of the incident proton, must all be visible. If the second scatter occurs near the top or bottom of the bubble chamber, for some azimuthal directions the protons may leave projected track lengths too short to be seen in the photographs. This forms a bias in polarization measurement. Each event must be corrected individually. Twelve percent of our events were affected. Eq. (1) then becomes

$$\mathcal{L}(P_0) \propto \prod_i^k \left[(1 + P_0 P_{1_i} \cos \phi_i) \Big/ \int_{\phi_{1_i}}^{\phi_{2_i}} (1 + P_0 P_{1_i} \cos \phi) d\phi \right], \qquad (2)$$

where ϕ_{1_i} and ϕ_{2_i} are the limits of visibility on the ith event.

The analyzing power assigned in the preceding sections must be multiplied by the cosine of the angle between the normals to the first and second scattering planes. These normals are defined by the cross products

$$\hat{n}_1 = \frac{\underset{\sim}{P}_{K_{in}} \times \underset{\sim}{P}_{p_{0_1}}}{\left| \underset{\sim}{P}_{K_{in}} \times \underset{\sim}{P}_{p_{0_1}} \right|}; \quad \hat{n}_2 = \frac{\underset{\sim}{P}_{p_{0_2}} \times \underset{\sim}{P}_{p_{sc}}}{\left| \underset{\sim}{P}_{p_{0_2}} \times \underset{\sim}{P}_{p_{sc}} \right|}; \quad \cos \Phi = \hat{n}_1 \cdot \hat{n}_2 . \qquad (3)$$

This assumes that neither the proton's velocity nor spin has been disturbed between scatters. The normals $\hat{n}_1$ and $\hat{n}_2$ are defined in terms of the momenta of the incident K^+, $[\underset{\sim}{P}_{K_{in}}]$, of the recoiled proton at the first scatter $\underset{\sim}{P}_{p_{0_1}}$, of the incident proton at the second scatter $\underset{\sim}{P}_{p_{0_2}}$, and of the scattered proton at the second scatter $\underset{\sim}{P}_{p_{sc}}$. The terms $\hat{n}_1$ and $\hat{n}_2$ are the orientations along which polarizing and analyzing of the proton spin can occur. Cosine Φ gives the projection of $\hat{n}_1$ on $\hat{n}_2$.

Generally $\underset{\sim}{P}_{P0_1}$ is set equal to $\underset{\sim}{P}_{P0_2}$, since both quantities refer to the same particle, but we must consider the effects of the magnetic field and of the medium (propane) on the spin orientation of the proton before we can do this.

The magnetic field $\underset{\sim}{B}$ causes spin precession separately about the direction of $\underset{\sim}{B}$ and about the velocity direction, $\underset{\sim}{v}$. The vector $\underset{\sim}{v}$ itself changes orientation at the cyclotron frequency as the proton moves in the field.

The medium slows down the proton and also may cause some depolarization. The slowing down affects both the spin precession and the rotation of the velocity vector. It also affects the analyzing power since this is momentum dependent.

The spin precession formula used is due to G. W. Ford.[18]

$$\underset{\sim}{\omega}_0 = \frac{e\,\underset{\sim}{B}}{m\gamma c}\left[1 + \left(\frac{g}{2} - 1\right)\gamma\right] - \frac{\underset{\sim}{v}}{|\underset{\sim}{v}|}(\gamma - 1)\left(\frac{g}{2} - 1\right)\left[\left(\frac{e\,\underset{\sim}{B}}{m\gamma c}\right)\cdot\left(\frac{\underset{\sim}{v}}{|\underset{\sim}{v}|}\right)\right].$$

We have neglected the second term, the precession component about the velocity. We estimate the error caused by neglecting the second term to be 10% and so comparable to the error due to the variation of magnitude of B over the chamber.

Neglecting the effect of the proton-energy loss on the spin precession causes an underestimation of precession angle by at most 12%. All these effects give less than an 8-deg uncertainty in ϕ, which is well within statistical uncertainties.

Depolarization of protons does occur to some extent,[16] but no complete information covering a wide range of energies and angles is available (triple scattering experiments are needed to give this information). We have not

included this correction, and have therefore underestimated the polarization by some unknown factor.

The analyzing power has been adjusted to the calculated momentum loss.

We now state the results of the application of Eq. 2 to the four intervals of $\theta_K^{c.m.}$ chosen on the basis of the distribution shown in Fig. 6:

$$\overline{P}_0 (\ 40 \leq \theta_K^{c.m.} < 70 \text{ deg}) = -0.80 \pm 0.80 ,$$

$$\overline{P}_0 (\ 70 \leq \theta_K^{c.m.} < 100 \text{ deg}) = -0.74 \pm 0.45 ,$$

and

$$\overline{P}_0 (100 \leq \theta_K^{c.m.} < 140 \text{ deg}) = +0.55 \pm 0.93 ,$$

$$\overline{P}_0 (140 \leq \theta_K^{c.m.} < 160 \text{ deg}) = +0.70 \pm 0.93 .$$

The corresponding curves, with the logarithm of $\mathcal{L}(P_0)$ plotted vs P_0, are shown in Figs. 7a, b, and d. The sign conventions have been chosen to conform to the conventions used in the subsequent phase-shift analysis and can be summarized as follows:

Positive analyzing power means that protons with spin "up" will scatter to the left in the second scatter. The sign of the polarization is defined to be positive when the majority of the protons recoiling to the left of the incident K^+ meson had their spin vectors "up." Thus, positive polarization corresponds to a majority of the events having $\cos \phi_i = +1$ in Eq. (1).

VI. PHASE-SHIFT ANALYSIS

The analysis of our angular distribution into phase-shift solutions incorporating the polarization data was performed by a computer program called KAPANAL, written by Dr. J. H. Foote and thoroughly described in his thesis.[21]

This program was a least-squares grid-search system to find a set of phase shifts that would give a minimum value of χ^2 for the experimental data,

starting from a set of random numbers. One can start the minimization procedure over and over again with new sets of random numbers, thus eventually covering most of the χ^2 surface. The program has been adapted by Dr. Victor Cook, as is described in his thesis,[4] and in the work of Cook et al.[5]

In the input data, other than the random numbers that form the starting point of the calculation, the following must be included: the ten differential cross-section points from the angular distribution (Fig. 4), the four measured values of the differential polarization, $\overline{P}_0(\theta)_K^{c.m.}$, a total cross-section estimate, and a total elastic cross-section normalization estimate.

The last two items were obtained from other experiments in neighboring energy regions[3,4] by interpolation. No exhaustive attempt was made to measure cross sections, though a means was adopted to see that our data corroborated the conclusions of the other experiments. This involved a tau-decay scan[15] which gave the K^+ beam flux and showed that our total elastic cross section was within one standard deviation of the extrapolated value used in the program.

The cross sections used were:

$$\sigma_{(\text{total})} = 14.7 \pm 1.3 \text{ mb}, \quad \text{and} \quad \sigma_{(\substack{\text{total} \\ \text{elastic}})} = 11.8 \pm 1.9 \text{ mb}.$$

From the cosine-series fit to the angular distribution, we see that the term of highest degree is $\cos \theta_K^{c.m.}$ or, possibly, $\cos^2 \theta_K^{c.m.}$. Thus, one would expect the p-wave to be the highest angular-momentum state needed to describe the interaction.

Yet, following the reasoning of Cook et al.,[5] we also allowed for a $D_{3/2}$ interaction since this corresponds to a possible N^* formation channel:

$$K^+ + p \rightarrow K + N^* \rightarrow K + N + \pi .$$

(Threshold momentum is 880 MeV/c.) If one assumes the N^* production to take place in an orbital (K^+, N^*) S state, the $\frac{3}{2}$ + spin-parity assignment of the N^* requires the K^+, p system to have been in a $D_{3/2}$ state.

Recently Kehoe[15] has shown that the inelastic process

$$K^+ + p \rightarrow K^0 + p + \pi^+$$

at 910 MeV/c can be completely described if we assume the π^+ and proton are the decay products of the $J = 3/2$, $I = 3/2$ N^* that was produced by the exchange of a ρ meson.[22] The 2.1 ± 0.2-mb cross section reported for this process represents a major part of the inelastic cross section at this energy.

We made several attempts to include the absorption in all momentum channels and found in each case, however, that the clustering of solutions (on which we depend to discern the shape of the χ^2 surface) is smeared into a broad, general background. The same phenomenon, though less severe, occurred upon inclusion of the absorption in only two channels.

It was decided, therefore, to limit absorption to one channel, though giving each channel the same number of random trials. Stubbs et al.[3] had made the same decision and had found the results insensitive as to which channel was chosen.

Four hundred sets of solutions were obtained. There were 300 trials in the "S and P" category (100 for each of the three ways of including the absorption) and 100 trials of the "S-P-$D_{3/2}$" category. The first 50 trials in each category gave us nearly all the solutions; the last 50 brought these out

again plus only two new ones, which were the sign-changed solutions of some that had appeared previously. We concluded, therefore, that nearly all solutions had been found.

We obtained a χ^2 distribution whose shape fitted a theoretical curve very well. We chose a cutoff at $P(\chi^2) = 0.01$.

To test the validity of this cutoff, we went back to the likelihood function given by Eq. (2). In determining the polarization we maximized $\mathcal{L}(P_0)$ as a function of P_0. We now changed this procedure in the following way. We first identified all the clusters of similar solutions from the phase-shift fitting program, regardless of their χ^2 probability. Every solution predicts a differential polarization function $P_0(\theta_K^{c.m.})$. We then inserted for each of the 94 events ($i = 1, 2, \ldots 94$) its value of $[P_{0_j}(\theta_{K_i}^{c.m.})]$, as predicted by the jth solution ($j = 1, 2, \ldots 52$). Then $\mathcal{L}$ became the relative probability for the jth solution:

$$\mathcal{L}(\delta_{s_j}, \delta_{p_{1/2_j}}, \ldots) \propto \prod_i^k \left\{ \frac{\left[1 + P_{0_j}\left(\theta_K^{c.m.}\right) P_{1_i} \cos \Phi_i\right]}{\int_{\Phi_{1_i}}^{\Phi_{2_i}} \left[1 + P_{0_j}\left(\theta_K^{c.m.}\right) P_{1_i} \cos \Phi\right] d\phi} \right\}.$$

Likelihood rejection ratios can be set up. We considered that a ratio of 250:1 was sufficient to dismiss a particular solution.

This procedure is not independent of the KAPANAL program since the same polarization information is used in both; yet, there is a difference. KAPANAL uses a "lumped" polarization $\overline{P}_0$ over an angular region. The likelihood method, on the other hand, uses each event individually. The sensitivity of these methods is different. We therefore used the one as a check on the other.

All of the solutions rejected by χ^2 considerations were also rejected under our 250:1 likelihood rejection ratio. This is an indication that our χ^2 cutoff did not allow spurious solutions to enter. On the other hand, two or three solutions well within our likelihood tolerance were rejected by χ^2. In such cases we let χ^2 decisions prevail.

There were 37 solutions left after the χ^2 test. Next, error estimates were sought to detect overlap of solutions.

As explained in Foote's thesis,[21] an error matrix involving the real parts of the phase shifts can be calculated by the KAPANAL program. This is based on an expansion of the χ^2 equation in a Taylor series at a minimum point where the first derivatives with respect to the parameters are zero.

Another procedure used in KAPANAL is denoted as AUX by Foote. It is an auxiliary method of determining the variances and serves as a check on the error-matrix calculation. Only one phase shift is varied at a time. The other phase shifts then adjust to obtain a new minimum of χ^2. The value of this method is that it gives a geometrical interpretation to the χ^2 minimization process as motion inside a quadratic well.[21] This also, however, makes the method much more sensitive to the quadratic hypothesis.

In addition to these two methods, we employed a third as a check since both of these depended on quadratic behavior. We sought the clusters of solutions we had found previously and determined the variation among the same phase shifts in a given cluster. This relies on the real meaning of deviation as linked to the repetition of the same experiment a large number of times.

All three methods corroborated each other's results. We adopted the values of deviations given by the error matrix.

Having found the rms errors in the phase shifts, we then eliminated the large amount of overlap in our 37 solutions. Two solutions were considered to be overlapping if they fell within 2 standard deviations of each other.

Another phenomenon had to be eliminated. Several strings of linked solutions, each about 1 standard deviation away from its neighbors, were found. They generally tended to some "best" solution at a low value of χ^2. In such cases, only the "best" solution, toward which all the others tended, was chosen. The linked chain was taken to describe a deep, but rough well, on the walls of which many spurious relative minima might appear.

Our final results consist of ten S- and P-wave solutions and six S, P, $D_{3/2}$ wave solutions. These are presented in Tables I and II.

The curve of predicted polarization $P(\theta_K^{c.m.})$ vs $\theta_K^{c.m.}$ for each of these solutions, along with the location of the four $\overline{P}_0$ measurements, is shown in Figs. 8a to e.

VII. DISCUSSION

The angular distribution shows, as might be expected, a behavior midway between the near isotropy given by Stubbs et al.,[3] at 810 MeV/c, and the more pronounced forward peaking given by Cook et al.,[4,5] at 970 MeV/c. In this sense, the three experiments, combined with the work of Cook et al.[4,5] at 1170 and 1970 MeV/c, form a continuous series with increasing momentum.

The polarization measurements are mainly hampered by a lack of events. That propane is a good analyzing medium was shown by Fowler and Birge[9] and by Whatley,[19] yet in the present experiment we have attempted to show in some detail all the relevant steps, including corrections and approximations, that are to be considered when polarization measurements are undertaken in a propane bubble chamber.

Turning now to the phase-shift sets of Table I, we consider first the S-P solutions. Set A^+, A^-, which is a $P_{1/2} - P_{3/2}$ mixture, was also found by Stubbs et al.[3] and by Cook et al.[4,5] Set B^+, B^-, B' represented our dominant S-wave solutions. Goldhaber et al.[1] found that negative S-wave phase shifts described their data from 140 MeV/c at least as far as the 640-MeV/c region. The δ_s decreased from -10 deg at 140 MeV/c linearly with momentum to -36 deg at 642 MeV/c. A δ_s of -47 deg was also one of the results of Stubbs et al.[3]

We found the following situation with respect to solutions with large negative δ_s. There were numerous solutions of this type, but they all overlapped with a separation of 1 or, at most, 2 standard deviations. The solution labelled A^+, and included as a $P_{1/2} - P_{3/2}$ mixture, was actually the solution of low χ^2 toward which all the linked solutions with negative δ_s tended. The opposite end of the chain is typified by solution B^- with its large errors. On the other hand, B' represents a solution that lies in the mid-point of the chain.

What this could mean is that the solutions with dominant $-\delta_s$ lie in a broad deep rough depression in the χ^2 surface with a minimum at $\delta_s = 0$. The conclusion might be drawn from this that the $K^+ - p$ interaction is no longer dominated by a repulsive S-wave phase shift, though we are prevented, probably by our large polarization errors, from seeing more positive indication of this.

Sets C^+, C^-, C' and D^+, D^- are various dominant $\delta_{P_{1/2}}$ solutions. Some of these may be Minami ambiguities of the B set, though ambiguities do not remain clearly identifiable in the presence of absorption. It is hard to link up these solutions with the low-energy behavior, though similar sets were found by Stubbs et al.[3] and Cook et al.[4,5]

The D-wave solutions are presented in the second portion of Table I. No linking of chains of similar solutions was observed.

In summary, then, the added polarization information raises a possibility that the dominant S-wave behavior of $K^+ - p$ elastic scattering might have been superseded by a $P_{1/2} - P_{3/2}$ mixture. On the other hand a D-wave solution such as F offers a way of linking more easily to results at lower energy and to the inelastic channels at this energy.

ACKNOWLEDGMENTS

The scanning effort of Mrs. Rho Ganow is gratefully acknowledged. We thank Dr. Victor Cook for his explanation of the contents and use of the KAPANAL program. We also thank Dr. R. Birge, Dr. R. Ely, Dr. D. Keefe, Dr. A. Kernan, Dr. P. Newcomb, and Professor W. M. Powell for helpful conversations.

The Data Handling Group did the kinematic reconstruction and constraints and thanks are due Mr. H. White and Mr. L. Shalz.

FOOTNOTES AND REFERENCES

* This work done under the auspices of the U. S. Atomic Energy Commission.

† Based on a thesis submitted by Warner Hirsch in partial fulfillment of the requirements for a Ph. D. in physics at the University of California. [Warner Hirsch, Elastic K^+-Proton Scattering at 910 MeV/c; Polarization of the Recoil Protons (Ph. D. Thesis), Lawrence Radiation Laboratory Report UCRL-10813, May, 1963 (unpublished)].

1. S. Goldhaber, W. Chinowsky, G. Goldhaber, W. Lee, T. O'Halloran, T. F. Stubbs, G. M. Pjerrou, D. H. Stork, and H. K. Ticho, Phys. Rev. Letters 9, 135 (1962).
2. T. F. Kycia, L. T. Kerth, and R. G. Baender, Phys. Rev. 118, 553 (1960).
3. T. F. Stubbs, H. Bradner, W. Chinowsky, G. Goldhaber, S. Goldhaber, W. Slater, D. M. Stork, and H. K. Ticho, Phys. Rev. Letters 7, 188 (1961).
4. V. Cook, K^+-Nucleon Interactions in the Momentum Range of 800 to 2900 MeV/c (Ph. D. Thesis), Lawrence Radiation Laboratory Report UCRL-10130, March 1962 (unpublished).
5. V. Cook, D. Keefe, L. T. Kerth, P. G. Murphy, W. A. Wenzel and T. F. Zipf, Phys. Rev. 129, 2743 (1963).
6. W. M. Powell, W. B. Fowler, and L. O. Oswald, Rev. Sci. Instr. 29, 874 (1958).
7. G. Goldhaber, S. Goldhaber, J. Kadyk, T. F. Stubbs, D. Stork, and H. Ticho, Separated K^+ Beams, Lawrence Radiation Laboratory Report Bev-483, February 1960 (unpublished).

8. H. S. White, S. S. Buckman, D. E. Hall, E. Hurwitz, L. B. Meissner, J. C. Smith, and F. R. Stannard, The FOG, CLOUDY, and FAIR Programs for Bubble Chamber Data Reduction, Lawrence Radiation Laboratory Internal Report (unpublished).

9. R. W. Birge and W. B. Fowler, Phys. Rev. Lefters 5, 254 (1960); The data in this reference, as greatly expanded by Dr. V. Z. Peterson, in UCRL-10622 describes elastic p-carbon interactions and degrees of inelasticity of p-carbon interactions up to a proton energy loss of 50 MeV.

10. The measured χ^2 distribution in bubble-chamber data is often found to be of correct shape but displaced too far toward higher values of χ^2. This is due to a general underestimation of measurement errors, and must be corrected before a cutoff limit can be meaningful. Our errors were underestimated by a factor of 1.22.

11. This minimum δ-ray energy is approximately 0.4 MeV, though straggling may cause variation in this. In propane, an electron of energy greater than 1.0 MeV will lose 1 MeV per centimeter.

12. Since there are four constraint equations, we can deliberately omit measuring the momentum of a bad track, use a constraint to supply it and still have three conditions left to impose on the event.

13. We wish to thank Mr. T. G. Schumann for carrying out this scan.

14. This assumes that the angular distribution of π^+, p is similar to that of K^+, p. Actually the π^+, p distribution is peaked forward more than the K^+, p at this energy [see J. A. Helland, T. J. Devlin, D. E. Hagge, M. J. Longo, B. J. Moyer, and C. D. Wood, Phys. Rev. Letters 10, 27 (1963)]. Compensation for this brings the maximum π^+ contamination up from 0.5% to 1.0%. However, our rescan with a δ-ray search reduces this again.

15. B. Kehoe, Phys. Rev. Letters 11, 94 (1963); also, proviate communication.

16. A. E. Taylor, Rept. Progr. Phys. 20 (1957).

17. Since the existence of this factor was first called to our attention by Malcolm Whatley,[16] we shall henceforth refer to it as the Whatley correction. A detailed explanation is complicated and can be found in reference 20, Appendix D.

18. D. F. Nelson, A. A. Schupp, R. W. Pidd, and H. R. Crane, Phys. Rev. Letters 2, 492 (1959).

19. M. Whatley, Polarization in K^+-P Elastic Scattering (Ph. D. Thesis), University of Wisconsin, 1962; also, Bull. Am. Phys. Soc. Ser. II, 8 No. 1, 21 (1963).

20. For a complete discussion of the geometric corrections and the spin precession correction, see W. Hirsch, Elastic K^+-Proton Scattering at 910 MeV/c: Polarization of the Recoil Protons (Ph. D. Thesis), Lawrence Radiation Laboratory Report UCRL-10813, May, 1963 (unpublished).

21. J. H. Foote, Scattering of Positive Pions on Protons at 310 MeV; Recoil Nucleon Polarization and Phase Shift Analysis (Ph. D. Thesis), Lawrence Radiation Laboratory Report UCRL-9191, September, 1960 (unpublished).

22. L. Stodolsky and J. J. Sakurai, Phys. Rev. Letters 11, 90 (1963).

FIGURE CAPTIONS

Fig. 1. An example of a K^+-p elastic scatter followed by a p-carbon elastic scatter.

Fig. 2. Laboratory scattering angles for K-p and π-p elastic scattering at 910 MeV/c.

Fig. 3. Perpendicular distance of events before constraint (in deg) from (a) the θ_K as θ_p theoretical curve, and (b) the θ_π as θ_p theoretical curve.

Fig. 4. Experimental angular distribution at 910 MeV/c. Fit "A" is $1 + 0.18 \cos\theta$ while Fit "B" is $1 + 0.20 \cos\theta + 0.18 \cos^2\theta$.

Fig. 5. Angular distribution of the proton for p-C and p-p scatters.

Fig. 6. Center-of-mass angular distribution of K^+ for elastic scatters used in polarization determination. The ordinate is as described in the text.

Fig. 7. (a) Logarithm of the likelihood function $\mathcal{L}(P_0)$ in the angular region $40 \leq \theta_K^{c.m.} < 70$ deg.

(b) Logarithm of the likelihood function $\mathcal{L}(P_0)$ in the angular region $70 \leq \theta_K^{c.m.} < 100$ deg.

(c) Logarithm of the likelihood function $\mathcal{L}(P_0)$ in the angular region $100 \leq \theta_K^{c.m.} < 140$ deg, and

(d) Logarithm of the likelihood function $\mathcal{L}(P_0)$ in the angular region $140 \leq \theta_K^{c.m.} < 160$ deg.

Fig. 8. (a) Differential polarization curves for the phase shift solutions listed in Tables I and II. The experimental points are shown on each curve.

(b) Differential polarization curves [see caption for Fig. 8(a)].

(c) Differential polarization curves [see caption for Fig. 8(a)].

(d) Differential polarization curves [see caption for Fig. 8(a)].

(e) Differential polarization curves [see caption for Fig. 8(a)].

Table I. Solutions involving S and P waves.

Designation	δ_s	$\delta_{p_{1/2}}$	$\delta_{p_{3/2}}$	η	σ_{inel} (mb)	$P(\chi^2)$
A^+	0.6 ± 2.0	-17.1 ± 1.8	29.8 ± 0.8	$\eta_s = 0.80$	1.8	0.58
A^-	- 5.5 ± 1.5	20.3 ± 2.2	-29.0 ± 1.0	$\eta_{p_{3/2}} = 0.90$	1.9	0.01
B^+	44.6 ± 3.8	-12.9 ± 7.4	2.5 ± 3.1	$\eta_{p_{3/2}} = 0.77$	4.1	0.22
B^-	-41.2 ±24.5	- 6.8 ±28.4	13.1 ±26.2	$\eta_{p_{3/2}} = 0.77$	4.1	0.22
B'	-27.0 ±13.3	-19.1 ±11.8	22.1 ± 3.6	$\eta_{p_{3/2}} = 0.75$	4.4	0.25
C^+	- 2.7 ± 2.5	48.0 ± 0.9	3.0 ± 1.0	$\eta_s = 0.67$	2.8	0.07
C^-	- 5.4 ± 1.8	-46.2 ± 1.2	5.5 ± 1.9	$\eta_{p_{3/2}} = 0.86$	2.6	0.14
C'	9.4 ± 2.0	-57.9 ± 7.0	15.2 ± 3.2	$\eta_{p_{1/2}} = 0.50$	3.9	0.63
D^+	8.3 ± 1.7	74.8 ± 2.9	5.5 ± 1.6	$\eta_{p_{1/2}} = 0.53$	3.8	0.45
D^-	- 5.6 ± 1.9	-62.7 ± 1.8	- 1.1 ± 1.8	$\eta_{p_{1/2}} = 0.65$	2.9	0.05

Table II. Solutions involving S, P, and $D_{3/2}$ waves.

Designation	δ_s	$\delta_{P_{1/2}}$	$\delta_{P_{3/2}}$	$\delta_{D_{3/2}}$	$\eta_{D_{3/2}}$	σ_{incl} (mb)	$P(\chi^2)$
E	23.7 ± 7.7	22.4 ± 7.5	1.2 ± 0.9	-23.1 ± 1.4	0.67	5.5	0.29
F	-23.9 ± 5.9	-24.0 ± 2.4	18.9 ± 2.8	- 4.0 ± 1.3	0.86	2.6	0.58
G^+	26.1 ± 3.9	- 5.1 ± 3.1	2.2 ± 1.3	-27.4 ± 2.3	0.77	4.1	0.50
G^-	-18.3 ± 2.2	4.6 ± 2.1	0.5 ± 1.2	29.3 ± 0.9	0.99	0.2	0.01
H^+	2.6 ± 2.9	-17.9 ± 2.6	28.8 ± 1.2	- 3.6 ± 1.4	0.84	3.0	0.29
H^-	5.0 ± 3.5	19.5 ± 2.2	-26.5 ± 1.3	6.0 ± 1.2	0.80	3.6	0.12

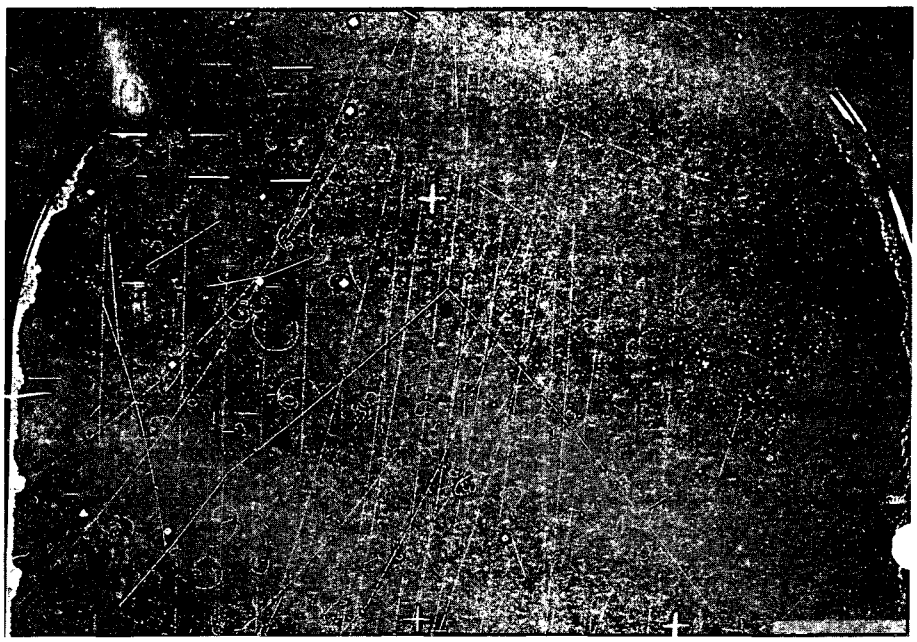

ZN-3820-A

Fig. 1.

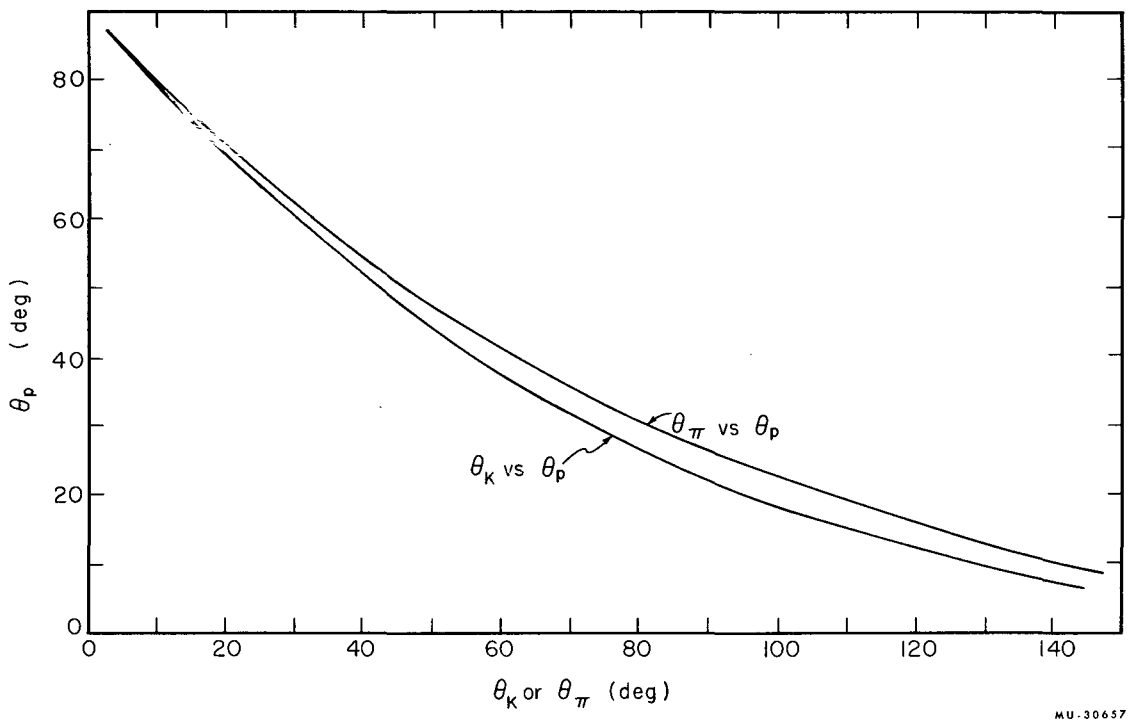
80
60
40
20
0
θ_p (deg)
0
20
40
60
80
100
120
140
θ_K or θ_π (deg)
θ_π vs θ_p
θ_K vs θ_p
MU-30657

Fig. 2.

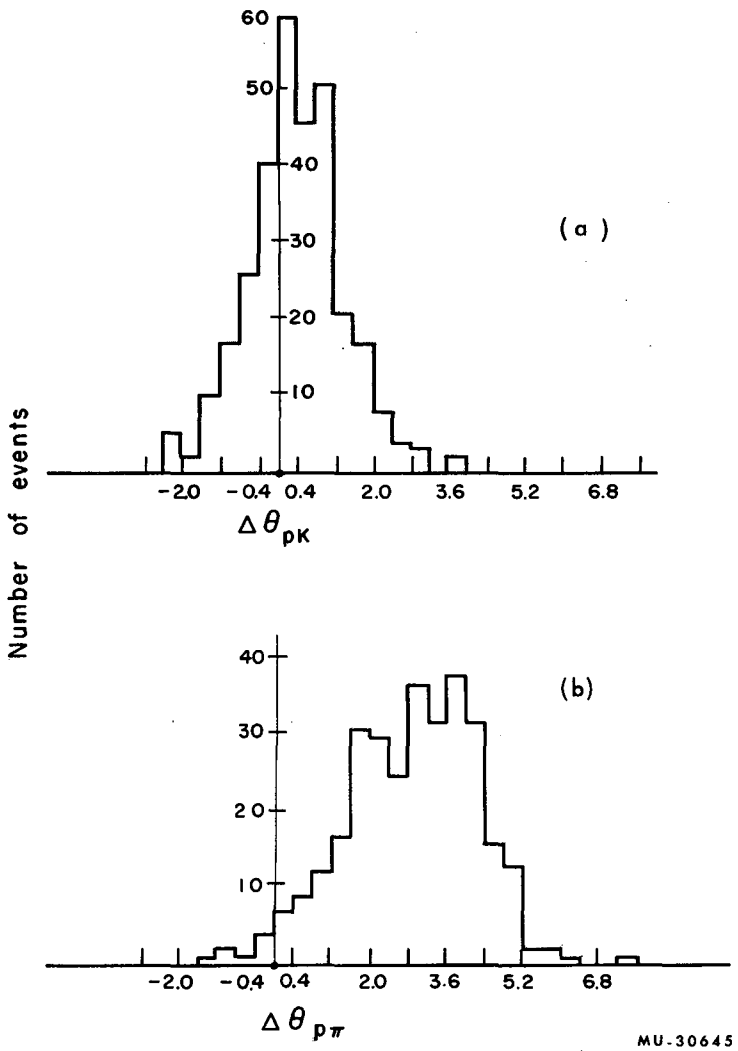
Number of events
60
50
40
30
20
10
(a)
-2.0
-0.4
0.4
2.0
3.6
5.2
6.8
Δθ pK
40
30
20
10
(b)
-2.0
-0.4
0.4
2.0
3.6
5.2
6.8
Δθ pπ
MU-30645

Fig. 3(a) and (b)

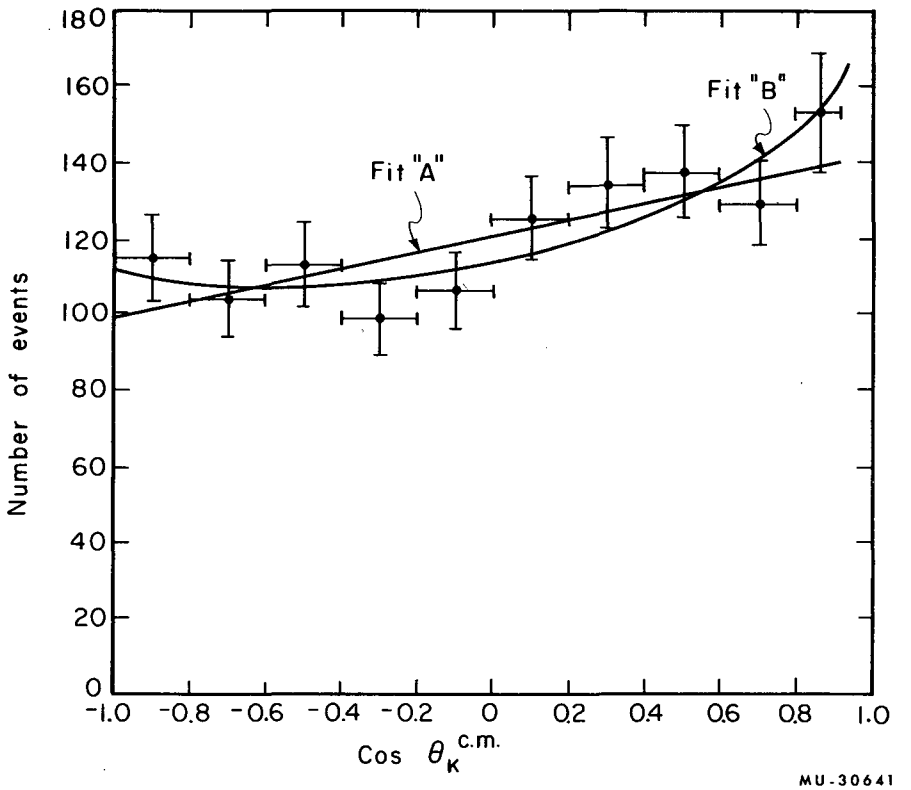
180
160
140
120
100
80
60
40
20
0
Number of events
Fit "A"
Fit "B"
-1.0
-0.8
-0.6
-0.4
-0.2
0
0.2
0.4
0.6
0.8
1.0
Cos $\theta_K^{c.m.}$
MU-30641

Fig. 4.

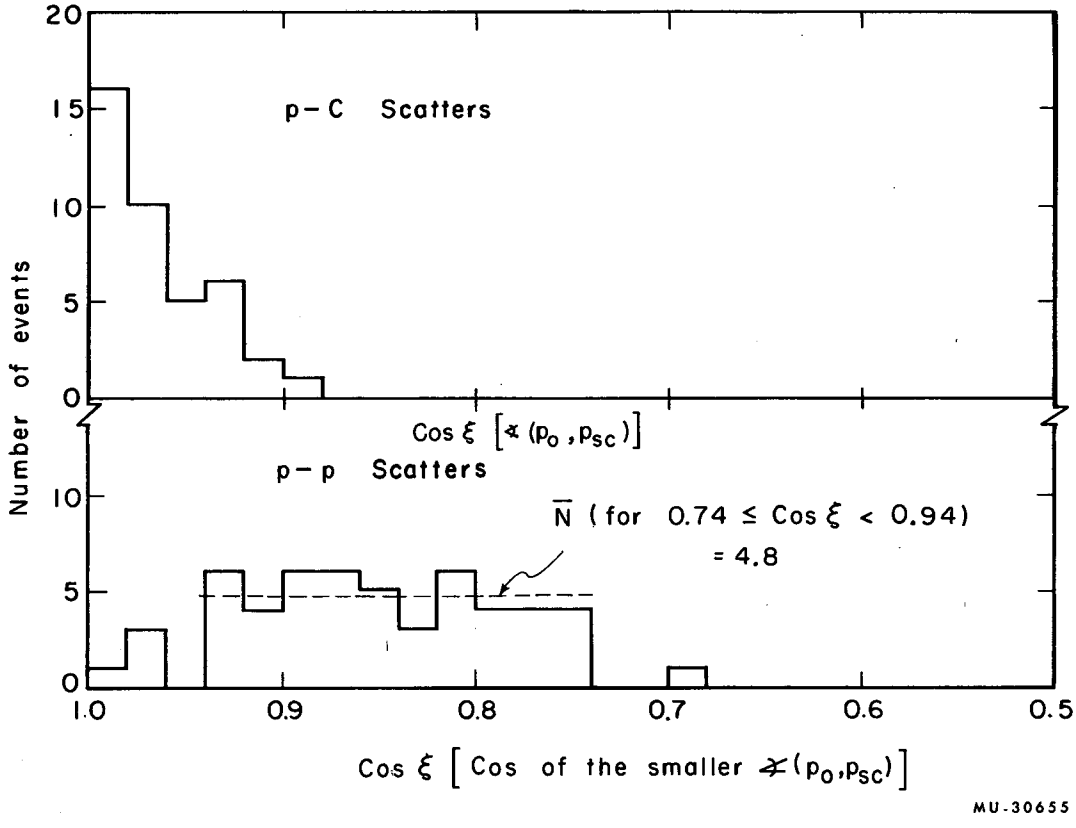
20
15
10
5
0
p – C Scatters
Number of events
Cos ξ [∢ (p0 , psc)]
p – p Scatters
10
5
0
N̄ (for 0.74 ≤ Cos ξ < 0.94)
= 4.8
1.0
0.9
0.8
0.7
0.6
0.5
Cos ξ [Cos of the smaller ∢(p0,psc)]
MU-30655

Fig. 5.

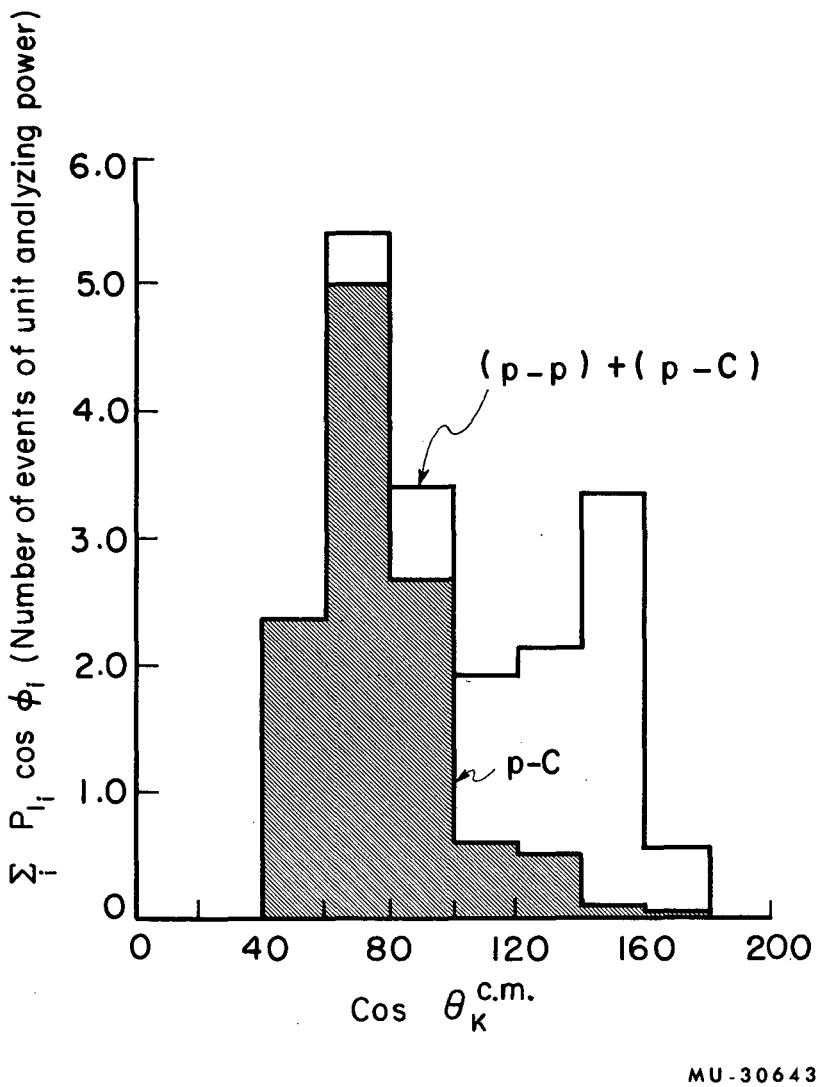
$\Sigma_i P_{1_i} \cos \phi_i$ (Number of events of unit analyzing power)
6.0
5.0
4.0
3.0
2.0
1.0
0
(p-p) + (p-C)
p-C
0
40
80
120
160
200
Cos $\theta_K^{c.m.}$
MU-30643

Fig. 6.

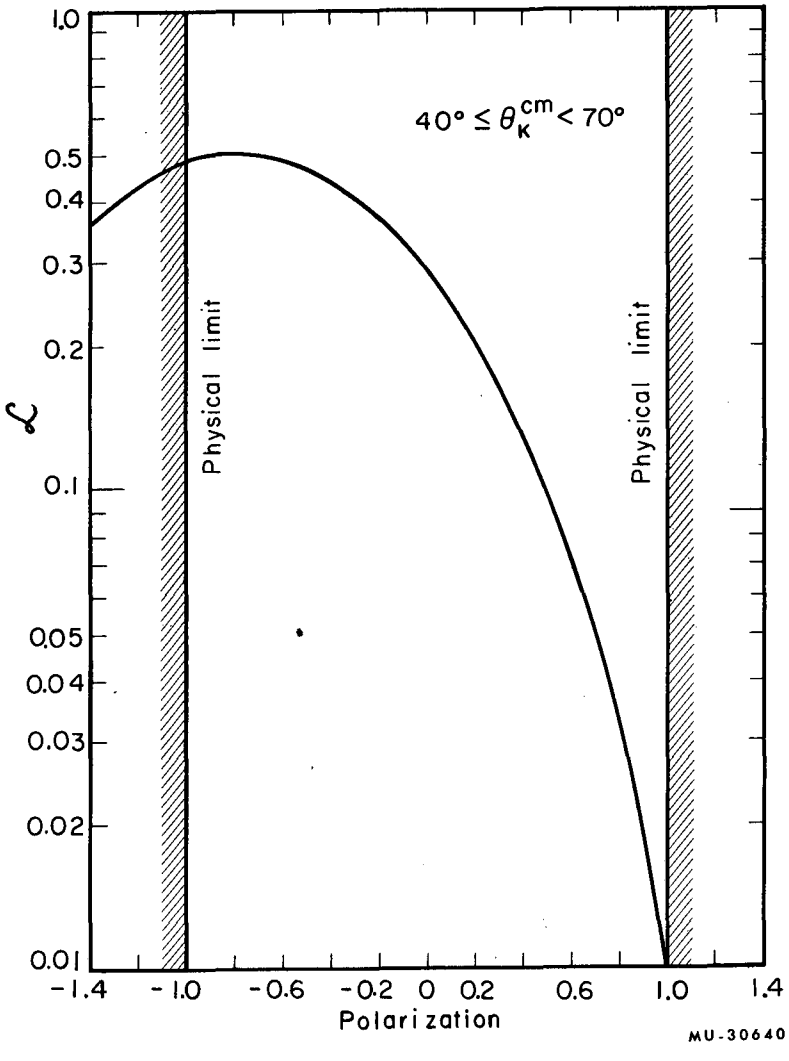
1.0
0.5
0.4
0.3
0.2
0.1
0.05
0.04
0.03
0.02
0.01
$\mathcal{L}$
$40° \leq \theta_K^{cm} < 70°$
Physical limit
Physical limit
-1.4
-1.0
-0.6
-0.2
0
0.2
0.6
1.0
1.4
Polarization
MU-30640

Fig. 7(a).

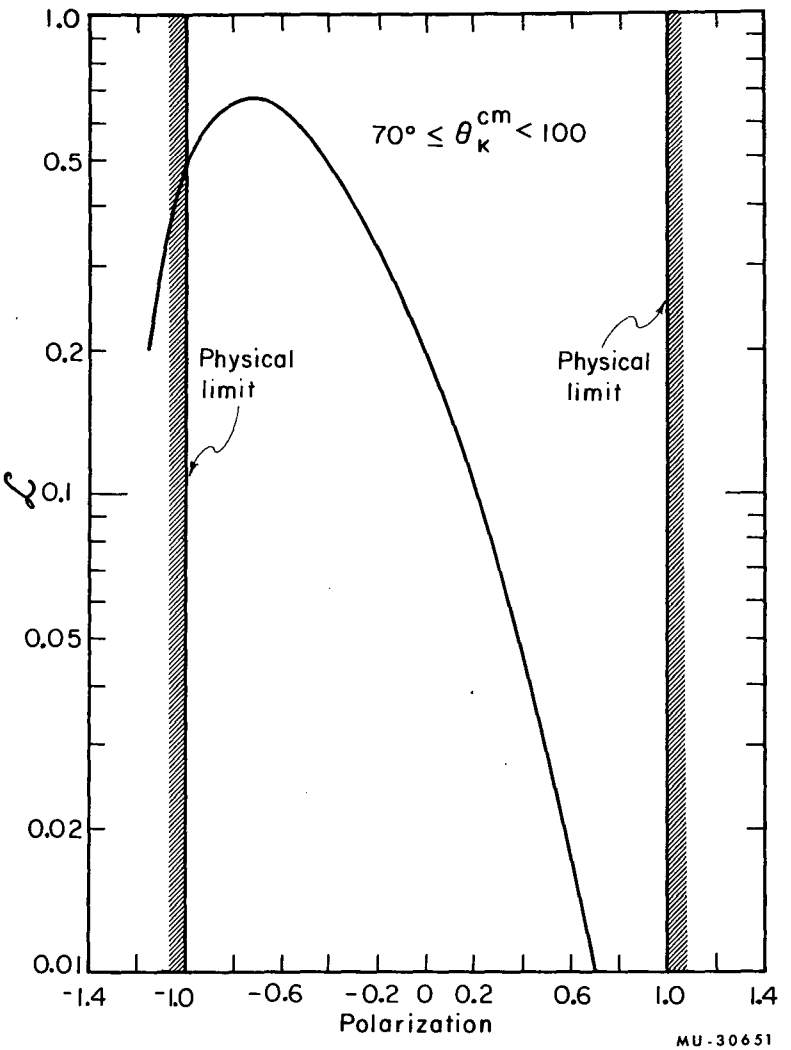
1.0
0.5
0.2
0.1
0.05
0.02
0.01
$70° \leq \theta_K^{cm} < 100$
Physical limit
Physical limit
-1.4
-1.0
-0.6
-0.2
0
0.2
0.6
1.0
1.4
Polarization
MU-30651

Fig. 7(b).

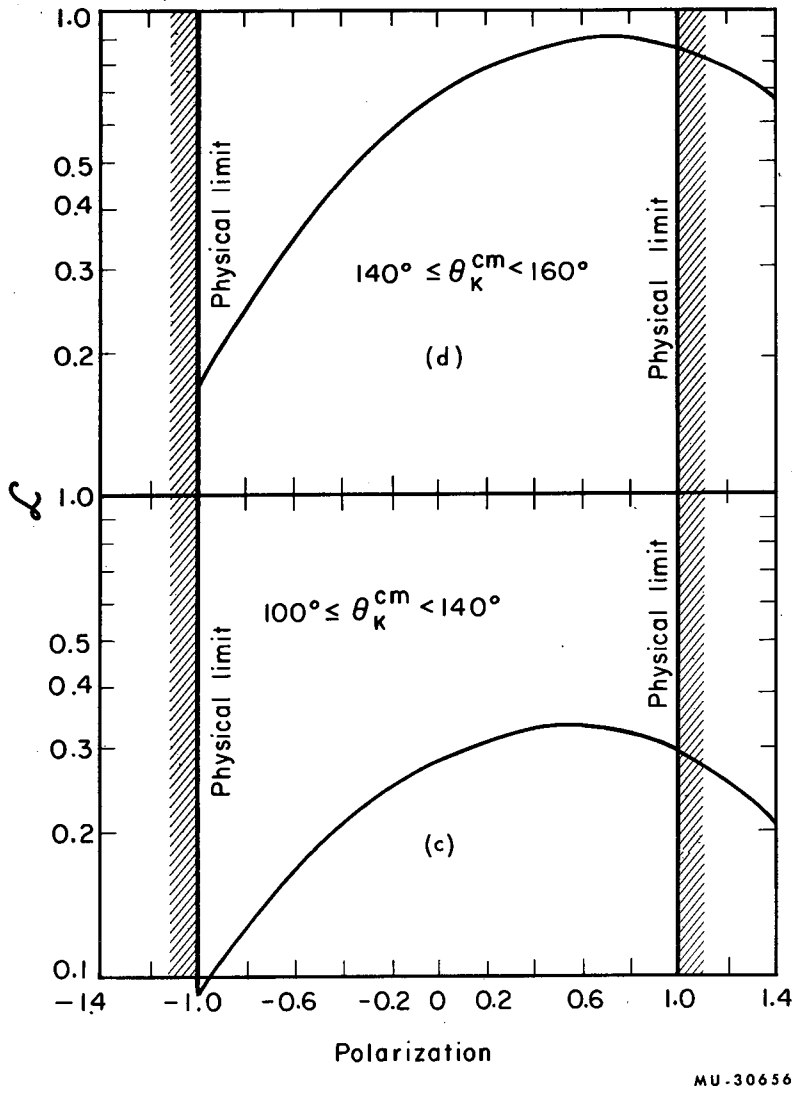
1.0
0.5
0.4
0.3
0.2
1.0
0.5
0.4
0.3
0.2
0.1
Physical limit
Physical limit
$140° \leq \theta_K^{cm} < 160°$
(d)
Physical limit
Physical limit
$100° \leq \theta_K^{cm} < 140°$
(c)
−1.4
−1.0
−0.6
−0.2
0
0.2
0.6
1.0
1.4
Polarization
MU-30656

Fig. 7(c) and (d).

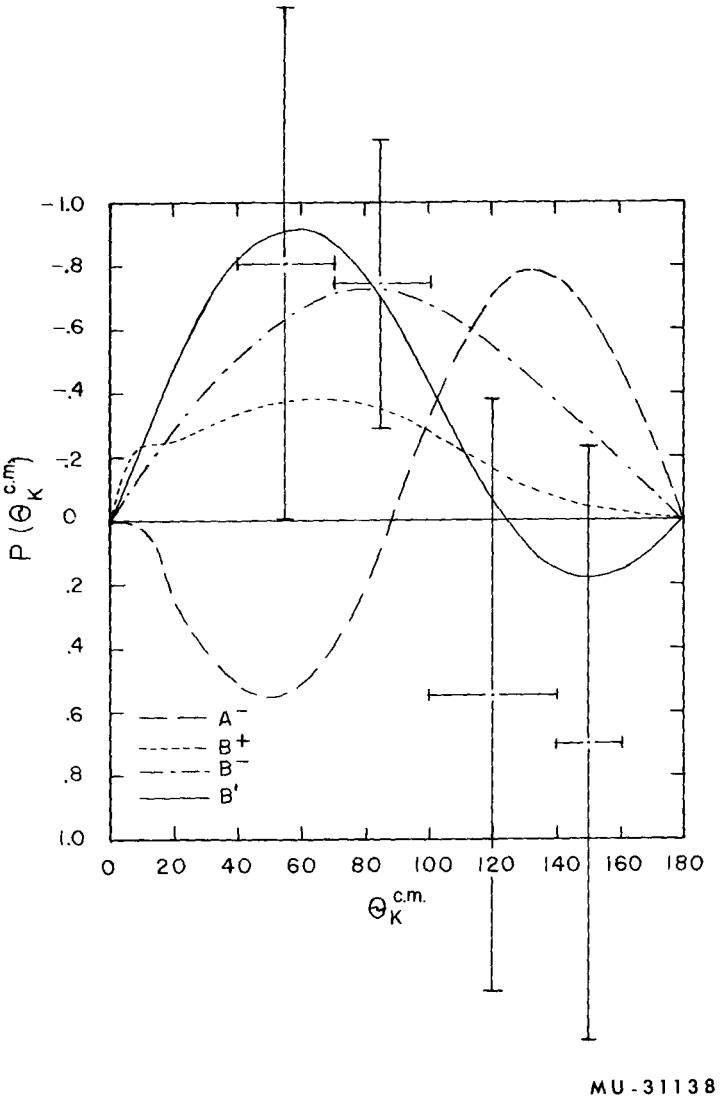
-1.0
-.8
-.6
-.4
-.2
0
.2
.4
.6
.8
1.0
P (Θ K c.m.)
A⁻
B⁺
B⁻
B'
0
20
40
60
80
100
120
140
160
180
Θ K c.m.
MU-31138

Fig. 8(a).

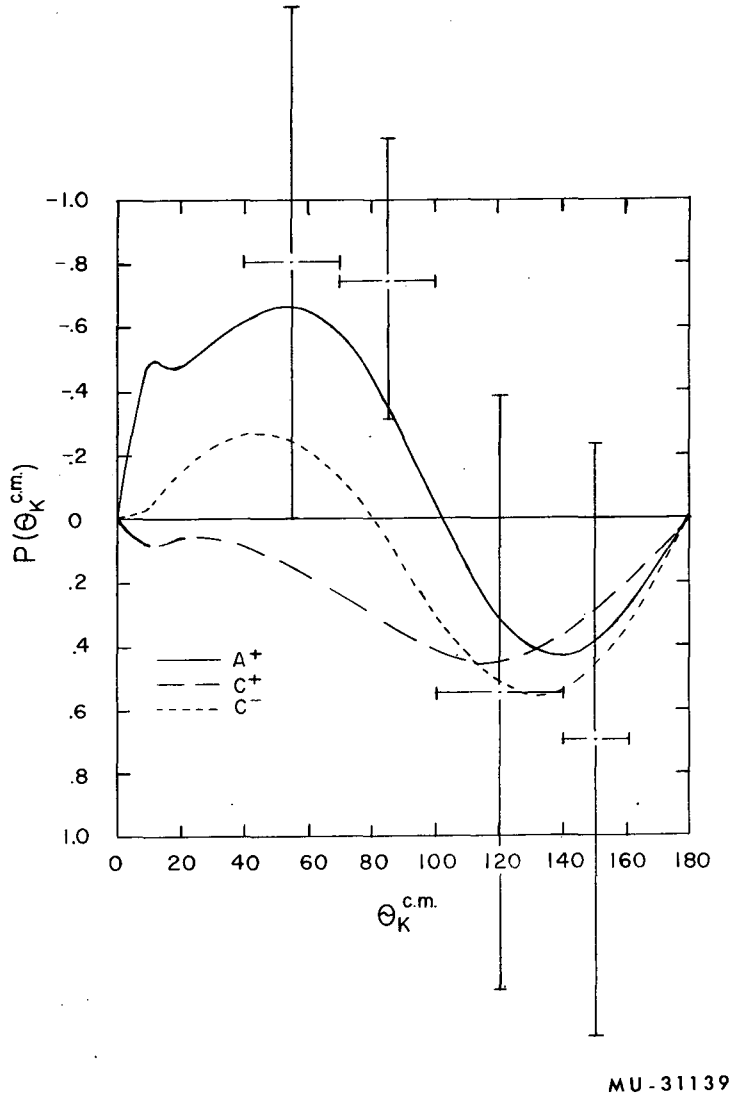
-1.0
-.8
-.6
-.4
-.2
0
.2
.4
.6
.8
1.0
P(Θ_K^c.m.)
A+
C+
C−
0
20
40
60
80
100
120
140
160
180
Θ_K^c.m.
MU-31139

Fig. 8(b).

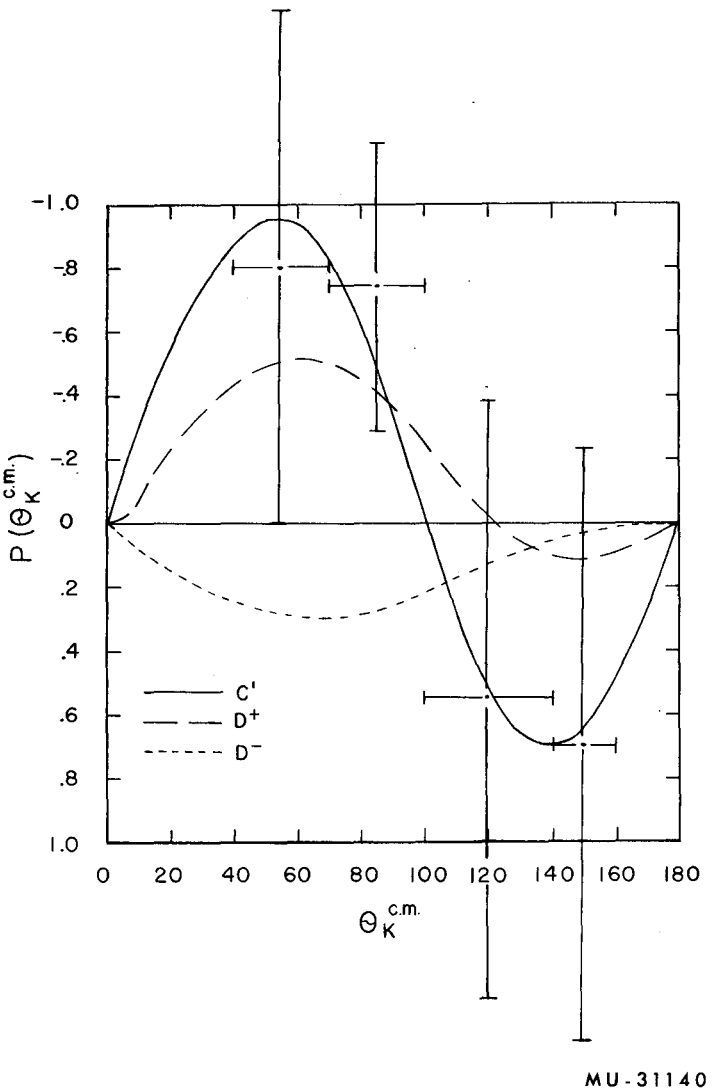
-1.0
-.8
-.6
-.4
-.2
0
.2
.4
.6
.8
1.0
P (Θ K c.m.)
C'
D+
D−
0
20
40
60
80
100
120
140
160
180
Θ K c.m.
MU-31140

Fig. 8(c).

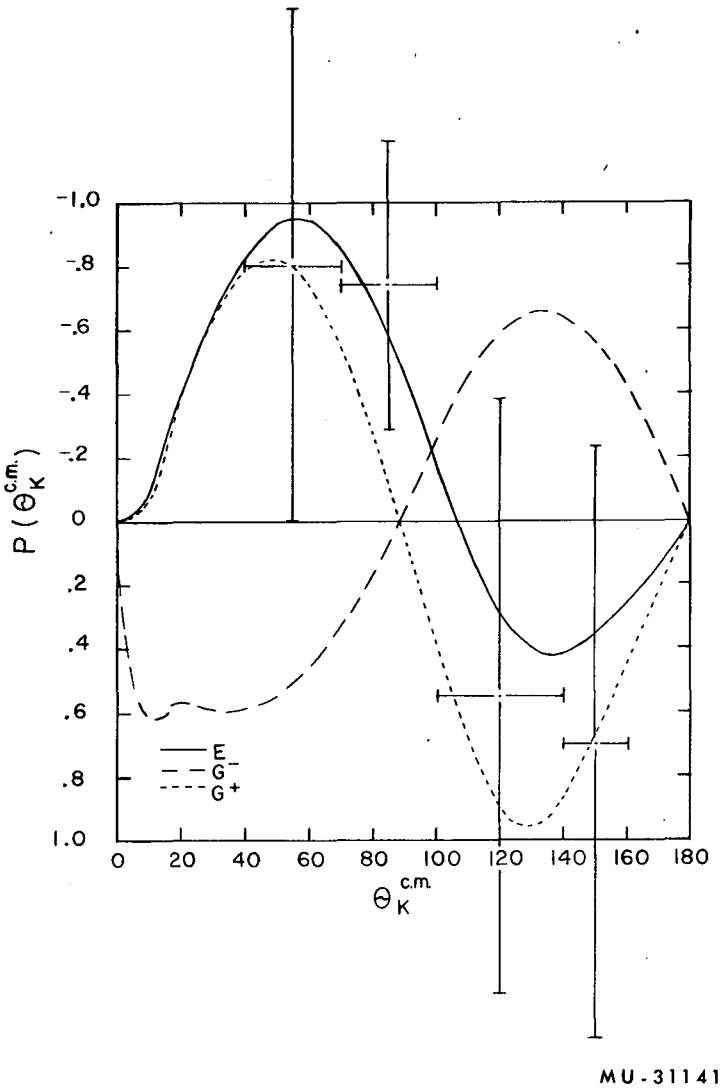
-1.0
-.8
-.6
-.4
-.2
0
.2
.4
.6
.8
1.0
P (Θ K c.m.)
E
G−
G+
0
20
40
60
80
100
120
140
160
180
Θ K c.m.
MU-31141

Fig. 8(d).

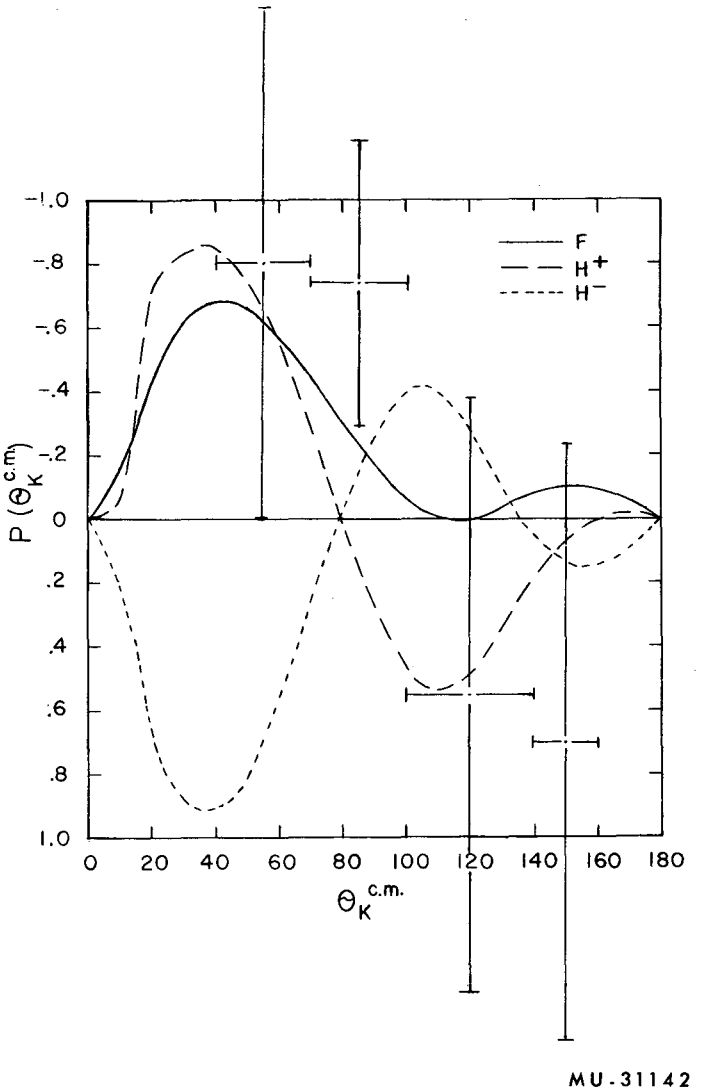
F
H+
H−
P (Θ K c.m.)
Θ K c.m.
-1.0
-.8
-.6
-.4
-.2
0
.2
.4
.6
.8
1.0
0
20
40
60
80
100
120
140
160
180
MU-31142

Fig. 8(e).